ACS APPLIED MATERIALS & INTERFACES

www.acsami.org

Research Article

Through Ring-Opening Reactions To Weaken the Hygroscopicity of PEDOT:PSS Films with Improved Stability of Silicon Hybrid Solar Cells

Yuzhou Liu,[§] Qi Geng,[§] Zhe Wang, Zhen Liu, Zhongliang Gao, Xin Sun, Yingfeng Li, and Meicheng Li*

Cite This: *ACS Appl. Mater. Interfaces* 2025, 17, 62022−62031

Read Online

ACCESS | Metrics & More | Article Recommendations | Supporting Information

ABSTRACT: Poly(3,4-ethylenedioxythiophene):poly(styrenesulfonate) (PEDOT:PSS), possessing excellent film-forming properties and high electric conductivity, is widely used in optoelectronic devices. However, the hygroscopicity of PSS results in progressive degradation of device performance during storage. Here, 4-*tert*-butylphenyl glycidyl ether was introduced as a reactive modifier into the PEDOT:PSS system to weaken the hygroscopicity of the PEDOT:PSS film. The ^{13}C NMR spectra confirmed the ring-opening reactions initiated by nucleophilic attack from the sulfonic acid groups in PSS. This reaction formed the new C−O bond between the carbon atom of the epoxy group and the oxygen atom of the sulfonic acid groups in PSS, successfully locking the hygroscopic sulfonic acid groups, thereby effectively weakening the hygroscopicity of the PEDOT:PSS film. Furthermore, the silicon hybrid solar cells were fabricated with modified PEDOT:PSS. It was found that, after 500 h of ambient air storage, the device retained 77% of the initial power conversion efficiency (PCE) of 12.31% compared to only 27% retention with the original PEDOT:PSS. This strategy provides a reference for developing stable and cost-effective optoelectronic devices utilizing PEDOT:PSS.

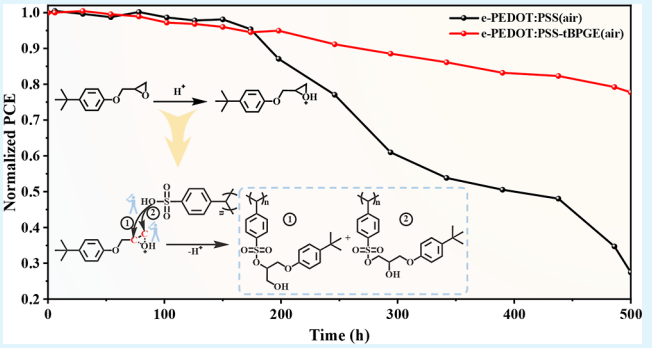

KEYWORDS: *PEDOT:PSS, 4-tert-butylphenyl glycidyl ether, Si, solar cells, ring-opening reactions*

1. INTRODUCTION

Poly(3,4-ethylenedioxythiophene):poly(styrenesulfonate) (PEDOT:PSS) has become a pivotal material in the energy area and the process of photovoltaic device fabrication[1−4] due to its high electric conductivity, transmittance, and favorable mechanical properties.[5−9] The polystyrene sulfonic acid (PSS) acts as a dispersing agent, resolving the solubility limitations of PEDOT.[10] However, in the PEDOT:PSS film, the sulfonic acid groups in PSS are prone to absorb moisture in air,[11−14] which degrades the long-term stability of photovoltaic devices based on this material. Therefore, weakening the hygroscopicity of the PEDOT:PSS film is crucial for developing stable optoelectronic devices.

To minimize the impact of water molecules in air on PEDOT:PSS film properties, numerous optimization strategies have been reported. For example, a copper iodide (CuI) overlayer was deposited on the PEDOT:PSS film to effectively reduce water absorption of the PEDOT:PSS film. The results indicated that the CuI-coated device retained 65% of its initial efficiency after storage in air for 300 h, compared to below 10% retention without a CuI layer.[15] Furthermore, a protective diethyl phthalate (DEP) layer was deposited on PEDOT:PSS/Si hybrid solar cells via the coating method, effectively preventing moisture adsorption by PSS. The DEP-treated devices exhibited merely 10% efficiency degradation after storage in air for 300 h.[16] On the other hand, doping PEDOT:PSS with waterborne acrylic resin (WA) formed a hydrophobic PEDOT:PSS film, achieving a water contact angle of 100.6° on the PEDOT:PSS film surface. Compared to a device without WA doping, the WA-doped photovoltaic device retained 80% efficiency after storage in air for 200 h.[17] Similarly, doping PEDOT:PSS with isobutyltriethoxysilane (IBTEO) could prepare a hydrophobic PEDOT:PSS film, enabling 78% efficiency retention after storage in air for 300 h, relative to 7% retention without IBTEO.[18] The hydrophobic PEDOT:A film was fabricated via in situ synthesis with fluoropolymer to replace PSS. The PEDOT:A/Si hybrid solar cells retained 90% of the initial efficiency after storage in air for 300 h, in comparison with 60% retention by PEDOT:PSS/Si hybrid solar cells.[19] At present, most research focuses on

Received: July 29, 2025
Revised: September 22, 2025
Accepted: October 23, 2025
Published: October 30, 2025

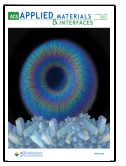

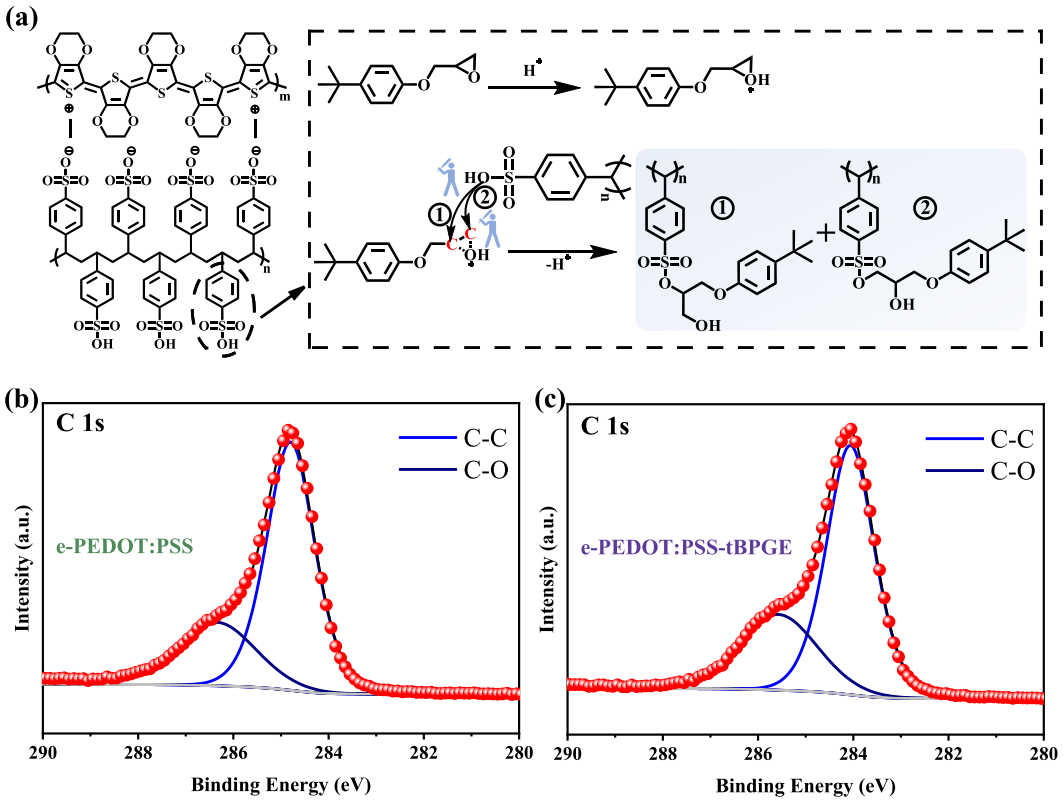

Figure 1. Mechanism of the ring-opening reaction and XPS spectra of the e-PEDOT:PSS film. (a) The mechanism schematic of the ring-opening reaction between e-PEDOT:PSS and *t*BPGE. (b) XPS spectra of C 1s of the e-PEDOT:PSS film and (c) with *t*BPGE doping.

enhancing the hydrophobicity of the PEDOT:PSS film. However, how to weaken the inherent hygroscopicity of the PSS component in PEDOT:PSS film is still neglected.

In this study, the PEDOT:PSS solution was prepared as an ethanol-dispersed PEDOT:PSS system. The hygroscopicity of PEDOT:PSS was weakened through nucleophilic ring-opening reactions between 4-*tert*-butylphenyl glycidyl ether (*t*BPGE) and the sulfonic acid groups in PSS. ^{13}C NMR spectra confirmed two distinct ring-opening pathways, and the formation of new C−O bonds was also found by the emergence of the sulfonate ester. The new C−O bond between the carbon atom of the epoxy group and the oxygen atom of the sulfonic acid groups in PSS successfully locks the hygroscopic sulfonic acid groups, which effectively weakens the hygroscopicity of the PEDOT:PSS film. Furthermore, *t*BPGE-doped PEDOT:PSS was used to construct Si hybrid solar cells. It was found that the environmental stability monitor demonstrated 77% efficiency retention after storage in ambient air for 500 h, compared to 27% retention without *t*BPGE.

2. EXPERIMENTAL SECTION

2.1. Material Preparation. Methanol-12C, d_4 was purchased from Adamas. Ethylene glycol (EG) (99%) and 4-*tert*-butylphenyl glycidyl ether (*t*BPGE) were purchased from Innochem. Dialysis membranes (500 Da) were bought from Yobios. A radial (100) polished single-side n-Si wafer was purchased from Tianjin Obode Technology Development Co., Ltd., with resistivity of 2−4 Ω·cm and thickness of 500 μm. PEDOT:PSS aqueous dispersion was Clevios PH1000 of Heraeus. The aqueous dispersion of PEDOT:PSS was prepared as an ethanol-dispersed solution of PEDOT:PSS according to the literature.[20] PEDOT:PSS aqueous dispersion was transferred to the dialysis membrane, and the dialysis membrane was put in the beaker with ethanol, and the magnetic stirrer was used to assist dialysis for about 40 min. Then, equivalent ethanol was added to the resulting product, and the resulting solution was crushed with an ultrasonic cell crusher for 3 h. During the crushing process, the program was set to stop for 0.1 s every 5 s. Finally, the resulting solution was filtered and then crushed for 1 h to obtain an ethanol-dispersed solution of PEDOT:PSS (e-PEDOT:PSS).

2.2. Device Fabrication. The Si wafer was cut into 1 × 1 cm^2 by a laser dicing machine. And then the Si wafer was cleaned in acetone, ethanol, and deionized (DI) water for 10 min each, and the Si wafer was dried with nitrogen. After the cleaning process, hydrofluoric acid was used to remove the native oxide layer on the Si surface, and then it was cleaned with DI water. *t*BPGE (1.5 and 3 vol %) (volume ratio to e-PEDOT:PSS solution) was doped into e-PEDOT:PSS solution and stirred adequately for 30 min. Then, 7.5 vol % ethylene glycol (EG) was doped into the e-PEDOT:PSS solution and stirred adequately. The e-PEDOT:PSS solution was spin-coated on the Si wafer at 4000 rpm and annealed at 120 °C for 15 min. A Ag electrode was deposited onto the e-PEDOT:PSS film through a shadow mask by magnetron sputtering with a thickness of 200 nm. A Ag film was prepared as the rear electrode with a thickness of 100 nm.

2.3. Characterization. The solar simulator (Keithley 2400, AM 1.5G, 100 mW/cm^2) was used to test the current density and voltage (J−V) characteristics. The Enli technology QE-R test system was used to detect external quantum efficiency (EQE) spectra and reflectivity spectra. The morphology of the e-PEDOT:PSS film without and with *t*BPGE doping was characterized by scanning electron microscopy (SEM-SU8100). Raman spectra of the e-PEDOT:PSS film were tested on a Si substrate. X-ray photoelectron spectroscopy (XPS-Thermo Scientific) was used to measure the optoelectronic information on the e-PEDOT:PSS film and Si surfaces after the e-PEDOT:PSS film was removed. The ^{13}C NMR spectra were obtained by a nuclear magnetic resonance spectrometer (AVANCE NEO 400), and using methanol-12C, d_4 as a solvent. Fourier transform infrared (FTIR) spectra were obtained by a Fourier transform infrared spectrometer (Spectrum 3).

https://doi.org/10.1021/acsami.5c14719
ACS Appl. Mater. Interfaces 2025, 17, 62022−62031

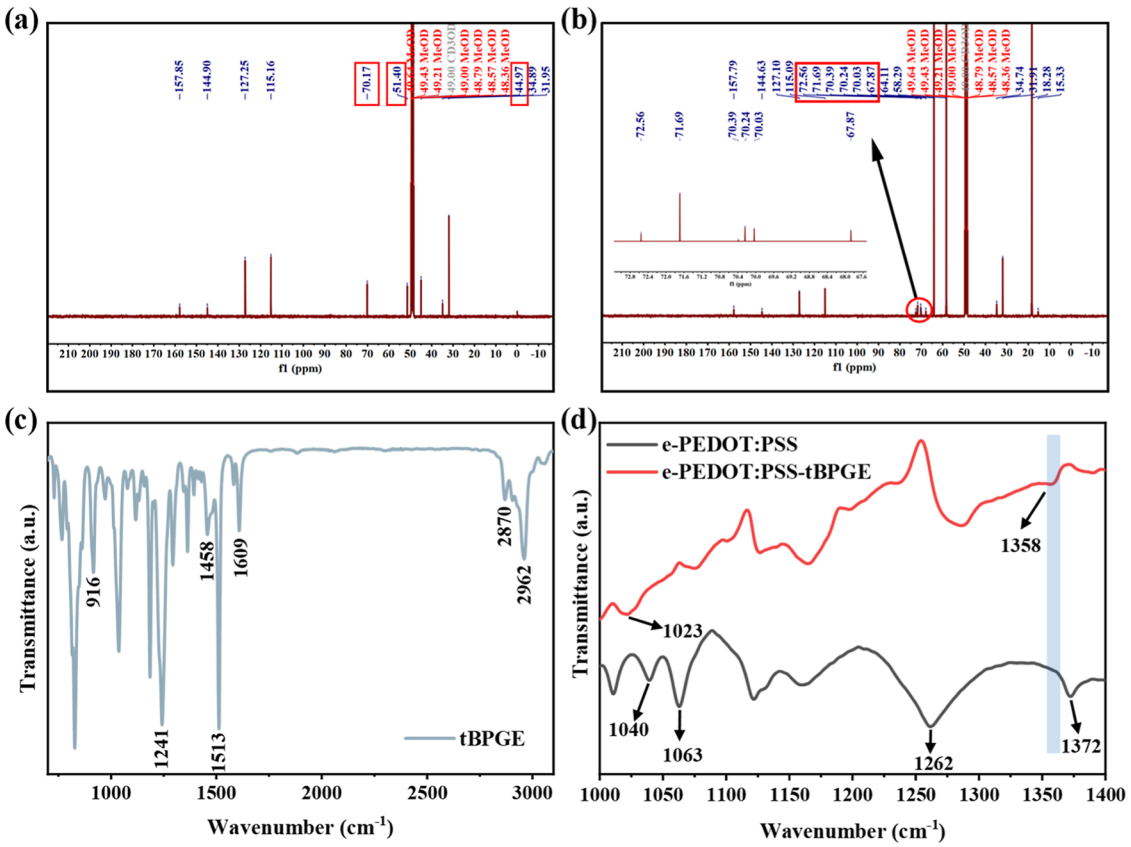

Figure 2. ^{13}C NMR spectra and FTIR spectra. (a) ^{13}C NMR spectra of *t*BPGE. (b) ^{13}C NMR spectra of *t*BPGE-doped e-PEDOT:PSS. (c) FTIR spectra of *t*BPGE. (d) FTIR spectra of the e-PEDOT:PSS film without and with *t*BPGE doping.

3. RESULTS AND DISCUSSION

3.1. The Hygroscopicity of the PEDOT:PSS Film. The hygroscopicity of PSS chains in the PEDOT:PSS film originates from sulfonic acid groups, which are hydrolyzed to generate sulfonate ions that adsorb water molecules, thereby degrading the performance of the PEDOT:PSS film.[12,21] This inherent moisture sensitivity of the PEDOT:PSS film limits the application of PEDOT:PSS in optoelectronic devices. To evaluate how the hygroscopicity of PEDOT:PSS films affects the performance of photovoltaic devices under different humidity conditions, the PEDOT:PSS/Si hybrid solar cells were constructed and exposed to a dry air atmosphere (less than 10% humidity) and ambient air (25% humidity), respectively. The normalized power conversion efficiency (PCE) variation with the time of the devices in different conditions is shown in Figure S1a. It was found that after 500 h, the device performance showed no significant degradation in a dry air atmosphere, while rapid degradation occurred in ambient air. In Figure S1b,c, we observed that the PCE degradation was primarily attributed to the fill factor (FF) attenuation, while the open circuit voltage (V_{OC}) and the short circuit current density (J_{SC}) remained stable from 0 to 500 h. The current−voltage (J−V) curves before and after 500 h are also shown in Figure S2, and after 500 h in ambient air, the devices exhibited a nearly S-shaped J−V curve in Figure S2a, whereas the J−V curve maintained appreciable rectangularity in a dry air atmosphere in Figure S2b. Finally, in Table S1, the devices retained 75% of the initial efficiency after storage in a dry air atmosphere for 500 h, compared to only 27% retention in ambient air, as shown in Table S2. Consequently, the hygroscopicity of the PEDOT:PSS film has an obvious impact on photovoltaic device performance. To overcome this challenge, we propose a strategy to weaken the hygroscopicity of the PEDOT:PSS film via the ring-opening reactions of epoxy compounds.

3.2. Elaboration of Ring-Opening Reactions. In Figure 1a, *t*BPGE is composed of a *tert*-butyl group, a phenyl group, an ether linkage, and an epoxy group. For epoxy groups, it easily undergoes ring-opening reactions by attack of nucleophilic reagents under acidic or alkaline conditions.[22,23] Although PSS is hygroscopic, considering the certain nucleophilicity of sulfonic acid groups in PSS, *t*BPGE was introduced to the PEDOT:PSS system. We found that the *t*BPGE is insoluble in water, but it has good solubility in ethanol, as shown in digital pictures of Figure S3a. Therefore, ethanol-dispersed PEDOT:PSS (e-PEDOT:PSS) was prepared. In Figure S3a,b, devices fabricated with e-PEDOT:PSS exhibited comparable performance to conventional PEDOT:PSS-based devices, and the specific electrical output parameters are also shown in Table S3. Although the PEDOT:PSS solution is prepared as ethanol-dispersed PEDOT:PSS, we believe that it also faces the problem of internal hygroscopicity due to the presence of sulfonic acid groups in PSS, which will affect the long-term stability of the device.

Thus, the *t*BPGE was introduced to the e-PEDOT:PSS solution, and the detailed reaction mechanism between *t*BPGE and e-PEDOT:PSS is shown in Figure 1a. First, under acidic conditions, it involves protonation of the epoxy group oxygen atom by H^+ generated from sulfonic acid groups hydrolysis in the e-PEDOT:PSS solution, which forms oxonium ions. This

https://doi.org/10.1021/acsami.5c14719
ACS Appl. Mater. Interfaces 2025, 17, 62022−62031

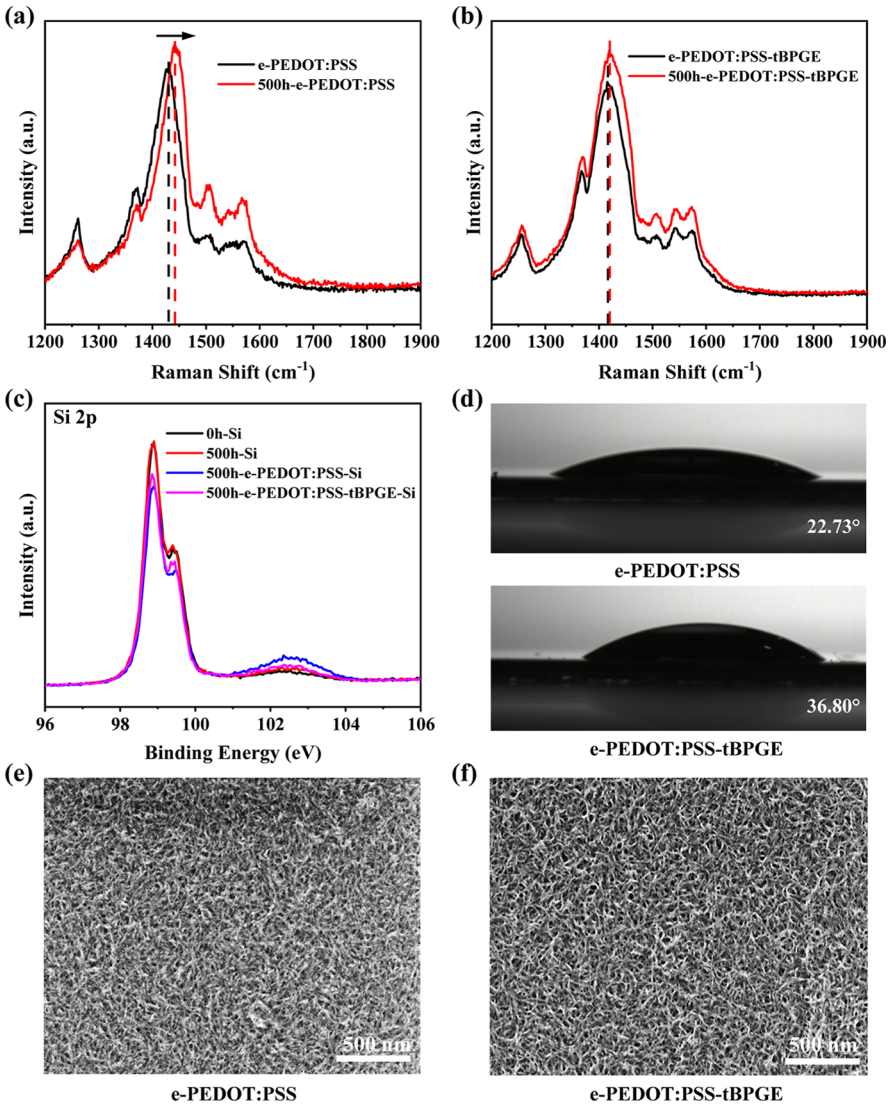

Figure 3. Raman and X-ray photoelectron spectroscopy (XPS) spectra, water contact angles, and surface scanning electron microscopy (SEM) images of different solutions and films. (a) Raman spectra of the e-PEDOT:PSS film without and (b) with *t*BPGE doping and stored in air for 500 h and freshly prepared. (c) XPS spectra of Si 2p collected from a bare Si wafer after 500 h air storage, Si wafer after 500 h air storage with undoped *t*BPGE film removed, Si wafer after 500 h air storage with doped *t*BPGE film removed, and freshly HF-etched Si wafer. (d) The contact angle of water on the e-PEDOT:PSS film without and with *t*BPGE doping. (e) SEM image of e-PEDOT:PSS films without and (f) with *t*BPGE doping on a Si surface.

weakens the C−O bond strength within the epoxy structure and enhances the susceptibility of adjacent ring carbon atoms attacked by nucleophilic reagents. Next, the sulfonic acid groups in PSS may attack both of the ring carbons of the epoxy structure, resulting in two distinct ring-opening pathways and their corresponding products, forming the new C−O bond between the carbon atom of the epoxy group and the oxygen atom of the sulfonic acid groups in PSS.[24] Meanwhile, X-ray photoelectron spectroscopy (XPS) analysis of the e-PEDOT:PSS film without and with *t*BPGE doping was performed, as shown in Figure 1b,c. A noticeable phenomenon is the increased proportion of C−O bonds, a 55.7% increase in the C−O/C−C peak area ratio from 0.307 to 0.478. The new C−O bond successfully locks the hygroscopic sulfonic acid groups, thereby effectively weakening the hygroscopicity of the PEDOT:PSS film.

In order to further verify that the C−O bonds were the result of the ring-opening reactions, ^{13}C NMR analysis was first tested, and all spectra were referenced to the CD_3OD at 49.00 ppm. Figure 2a shows the ^{13}C NMR spectrum of *t*BPGE, where the two peaks at 31.95 and 34.89 ppm can be observed belonging to the *tert*-butyl carbons of *t*BPGE. The phenyl carbons exhibited peaks between 115.16 and 157.85 ppm,[25] and the peak at 70.17 ppm corresponds to the ether carbon adjacent to oxygen in *t*BPGE. Peaks at 44.97 and 51.40 ppm belong to the carbons of the epoxy group.[26] Figure S4 shows the ^{13}C NMR spectra of e-PEDOT:PSS without *t*BPGE doping; we only found the peaks of the solvent of ethanol at 58.29 and 18.28 ppm and ethylene glycol at 64.10 ppm.[27] In Figure 2b, after introducing *t*BPGE into e-PEDOT:PSS, the peaks at 44.97 and 51.40 ppm disappeared, confirming that the epoxy groups undergo the ring-opening reaction. The peaks of the solvent peaks for ethanol and ethylene glycol do not change, which proves that they did not participate in the reaction. Meanwhile, six new peaks emerged at 72.56, 71.69, 70.39, 70.24, 70.03, and 67.87 ppm, proving two distinct ring-

https://doi.org/10.1021/acsami.5c14719
ACS Appl. Mater. Interfaces 2025, 17, 62022−62031

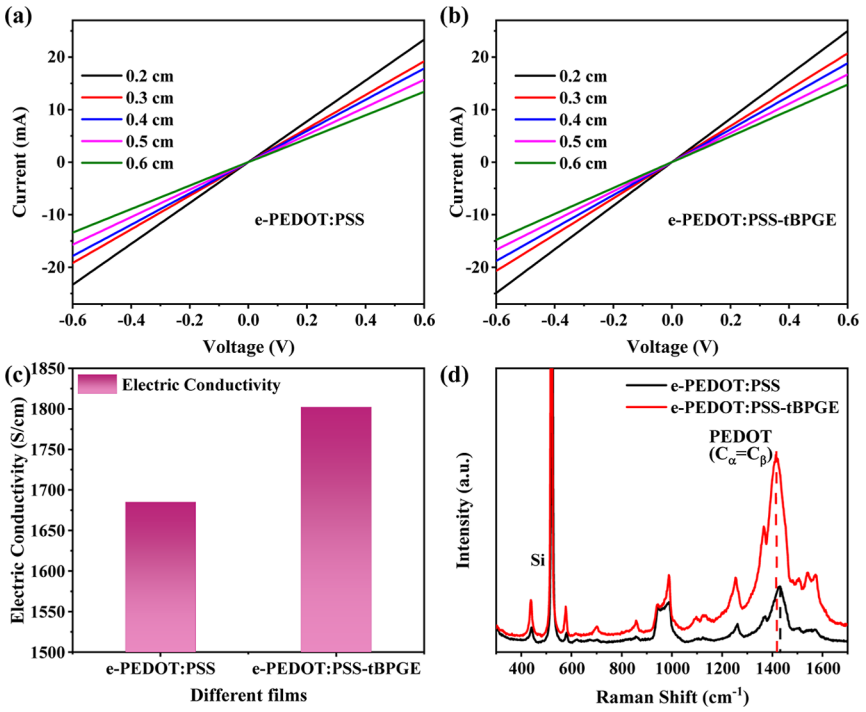

Figure 4. Electric conductivity and Raman spectra of e-PEDOT:PSS films without and with *t*BPGE doping. (a) Dark *I*−*V* characteristic curves of e-PEDOT:PSS films without and (b) with *t*BPGE doping on glass. (c) The value of the electric conductivity of different films. (d) Raman spectra of different films.

opening pathways. Each pathway yields three characteristic peaks consisting of two epoxide ring carbons and one adjacent carbon.

Furthermore, it was demonstrated that the newly formed C−O bond was between the carbon atom of the epoxy group and the oxygen atom of the sulfonic acid groups. The FTIR spectra of *t*BPGE and the *t*BPGE-doped e-PEDOT:PSS film are shown in Figure 2c,d. In Figure 2c, peaks at 1458, 1513, and 1609 cm^{-1} are attributed to the aromatic C═C stretch, and the peak of 1241 cm^{-1} corresponds to the C−O−C stretch in the aromatic ether group of *t*BPGE. Methyl and methylene groups are observed at the peaks of 2962 and 2870 cm^{-1}, while the peak at 916 cm^{-1} is ascribed to the epoxy group.[28−30]

In Figure 2d, the peak at 1372 cm^{-1} originates from the C−C and C═C stretch of the quinoidal structure of the thiophene ring,[31] and the peaks at 1262 and 1063 cm^{-1} are associated with the C−O−C stretch of PEDOT.[32] The peak at 1040 cm^{-1} is assigned to SO_3^- stretching of PSS.[33,34] After doping *t*BPGE with e-PEDOT:PSS, the disappearance of the epoxy group at 916 cm^{-1} is observed. Noticeably, the peak of SO_3^- exhibits a slight shift to a lower wavenumber from 1040 cm^{-1} to 1023 cm^{-1}, confirming that the sulfonic acid groups participate in the reaction. In addition, a new peak at 1358 cm^{-1}, which was the characteristic peak of the sulfonate ester[35] compound (−SO_2O−C−R), confirmed the formation of the new C−O bond between the carbon atom of the epoxy group and the oxygen atom of the sulfonic acid groups in PSS.

Based on the above analysis, the carbon atom of the epoxy group of *t*BPGE forms a C−O bond with the oxygen atom of the sulfonic acid group in PSS through a ring-opening reaction, thus weakening the hygroscopicity of the e-PEDOT:PSS film. To further verify the weakening of the hygroscopicity of the e-PEDOT:PSS film after *t*BPGE doping, Figure 3a,b shows the Raman spectra of e-PEDOT:PSS films without and with *t*BPGE doping stored in air for 0 and 500 h. We found that the peaks of the e-PEDOT:PSS film without *t*BPGE doping showed an obvious blue shift from 1430 to 1440 cm^{-1} after storage in air for 500 h. In contrast, the *t*BPGE-doped e-PEDOT:PSS film remained almost constant with only an extremely small blue shift under identical storage conditions. It has been reported in the literature[16] that this blue shift phenomenon is mainly due to the hygroscopicity of the PEDOT:PSS film. Furthermore, XPS was used to characterize the performance of the interface silicon oxide (SiO_X) layer. If a film deposited on a Si wafer exhibits hygroscopic behavior, it may accelerate the growth of SiO_X at the interface.[36−38] Figure 3c shows the XPS spectra of Si 2p of an HF-treated fresh Si wafer, a Si wafer after 500 h of storage in air, and a Si wafer after 500 h of storage followed by removal of e-PEDOT:PSS films (with and without *t*BPGE doping). The binding energy of about 102.5 eV was assigned to the SiO_X.[36] The peak intensity of SiO_X is the weakest for the fresh Si wafer treated with HF, while it is the strongest for the Si wafer after 500 h of storage, followed by the removal of the e-PEDOT:PSS film. The SiO_X peak intensities for both naturally oxidized and after removal of the *t*BPGE-doped e-PEDOT:PSS film are lower than pristine e-PEDOT:PSS. These observations demonstrate that the doping of *t*BPGE effectively suppresses SiO_X layer growth at the interface. After comprehensive analysis, the addition of *t*BPGE to the e-PEDOT:PSS solution resulted in the formation of new C−O bonds between the carbon atoms of the *t*BPGE epoxy group and the oxygen atoms of the sulfonic acid group in PSS due to ring-opening reactions, which indeed weaken the hygroscopicity of the e-PEDOT:PSS film.

Next, we further demonstrated that the above results are due to the weakening of the hygroscopicity of the e-PEDOT:PSS film by the ring-opening reaction and not realized by the enhancement of the hydrophobicity of the e-PEDOT:PSS film.

https://doi.org/10.1021/acsami.5c14719
ACS Appl. Mater. Interfaces 2025, 17, 62022−62031

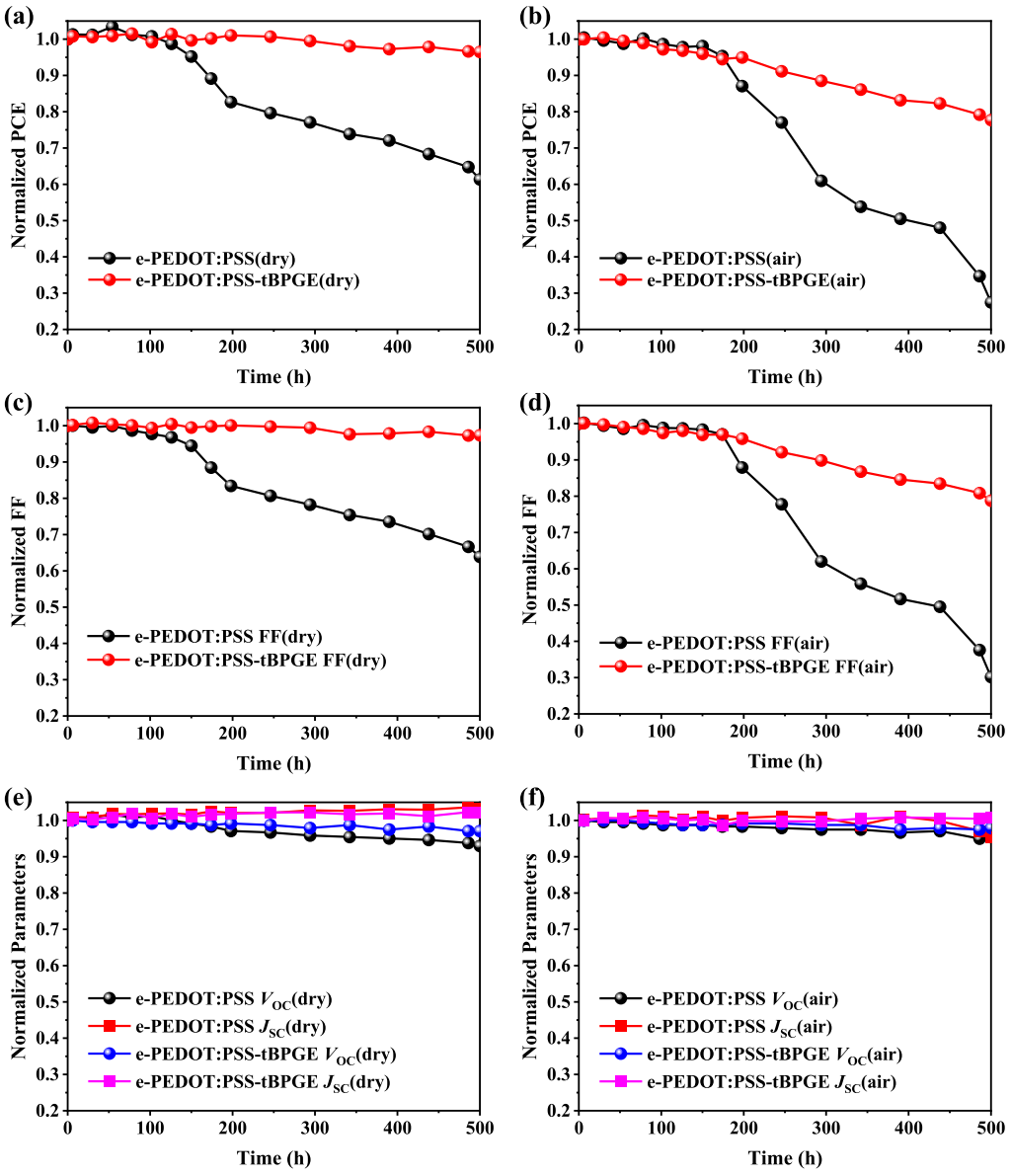

Figure 5. Normalized photovoltaic parameters varied with time of e-PEDOT:PSS/Si hybrid solar cells without and with *t*BPGE doping. (a) The normalized PCE varied with time in dry air and (b) ambient air. (c) The normalized FF varied with time in dry air and (d) ambient air. (e) The normalized V_{OC} and J_{SC} varied with time in dry air and (f) ambient air.

The contact angle of water on the e-PEDOT:PSS film surface is also shown in Figure 3d. The water contact angle without *t*BPGE doping was 22.73°, while the water contact angle was only slightly enhanced to 36.80° after the doping of *t*BPGE. However, this enhancement is not considered to be an enhancement of the hydrophobicity of the films compared to other studies where the water contact angle was upward of 100°. This also indicates that the slowing of the oxidation process on the silicon wafer surface was not achieved by enhancing the hydrophobicity of the e-PEDOT:PSS film surface. Instead, it was due to effectively weakening the hygroscopicity of the e-PEDOT:PSS film, thereby suppressing the growth of interfacial SiO_X. Furthermore, the surface morphology of the films was analyzed by scanning electron microscopy (SEM), as shown in Figure 3e,f. The results revealed that the surface morphology of the films was not changed between pristine and *t*BPGE-doped e-PEDOT:PSS films.

For materials used in optoelectronic devices, their conductivity is also crucial. To evaluate the electric conductivity of the films prepared with *t*BPGE doping, the electric conductivity of the films was assessed via the transmission line method (TLM). Figure 4a,b shows the dark $I-V$ characteristic curves of the e-PEDOT:PSS films without and with *t*BPGE doping for silver-grid line spacings from 0.2 to 0.6 cm. As the silver grid line spacing increases, the resistance of the film between the silver grid lines increases, and the current decreases. Therefore, the resistance of films with different widths can be calculated from Figure 4a,b, and the resistances obtained at different distances are fitted linearly as shown in Figure S5a,b. By linearly fitting the resistance obtained from different distances, the slope is the resistance per unit width of the film (ρ). It can be seen from Figure S5a,b that the ρ of e-PEDOT:PSS film without *t*BPGE doping is 45.099 Ω/cm, while the ρ of *t*BPGE-doped e-PEDOT:PSS film

https://doi.org/10.1021/acsami.5c14719
ACS Appl. Mater. Interfaces 2025, 17, 62022−62031

Table 1. Electrical Output Parameters of e-PEDOT:PSS/Si Hybrid Solar Cells without and with *t*BPGE Doping in a Dry Air Atmosphere[a]

type	J_{SC} (mA/cm^2)	V_{OC} (mV)	FF (%)	PCE (%)
e-PEDOT:PSS (dry)	27.43 (27.39 ± 0.48)	567.25 (568.17 ± 2.37)	72.39 (71.40 ± 1.60)	11.26 (11.11 ± 0.34)
500h-e-PEDOT:PSS (dry)	28.34 (27.96 ± 0.63)	527.45 (541.48 ± 10.35)	46.23 (47.69 ± 2.18)	6.91 (7.22 ± 0.44)
e-PEDOT:PSS-*t*BPGE (dry)	29.99 (30.18 ± 0.50)	562.55 (570.98 ± 5.25)	71.53 (70.85 ± 1.18)	12.06 (12.20 ± 0.09)
500h-e-PEDOT:PSS-*t*BPGE (dry)	30.60 (30.72 ± 0.54)	546.15 (553.65 ± 8.03)	69.67 (67.53 ± 2.05)	11.64 (11.48 ± 0.13)

[a]The statistical data are from five sets of solar cell data.

Table 2. Electrical Output Parameters of e-PEDOT:PSS/Si Hybrid Solar Cells without and with *t*BPGE Doping in Ambient Air[a]

Type	J_{SC} (mA/cm^2)	V_{OC} (mV)	FF (%)	PCE (%)
e-PEDOT:PSS (air)	28.77 (28.50 ± 0.34)	562.55 (562.07 ± 4.29)	70.89 (70.30 ± 1.03)	11.47 (11.26 ± 0.30)
500h-e-PEDOT:PSS (air)	27.44 (27.36 ± 0.95)	536.8 (545.69 ± 8.29)	21.38 (21.13 ± 2.03)	3.15 (3.17 ± 0.43)
e-PEDOT:PSS-*t*BPGE (air)	30.20 (30.10 ± 0.33)	567.25 (567.70 ± 3.09)	71.86 (71.21 ± 0.67)	12.31 (12.16 ± 0.13)
500h-e-PEDOT:PSS-*t*BPGE (air)	30.43 (30.38 ± 0.30)	555.50 (558.80 ± 6.39)	56.60 (55.36 ± 0.93)	9.57 (9.40 ± 0.13)

[a]The statistical data are from five sets of solar cell data.

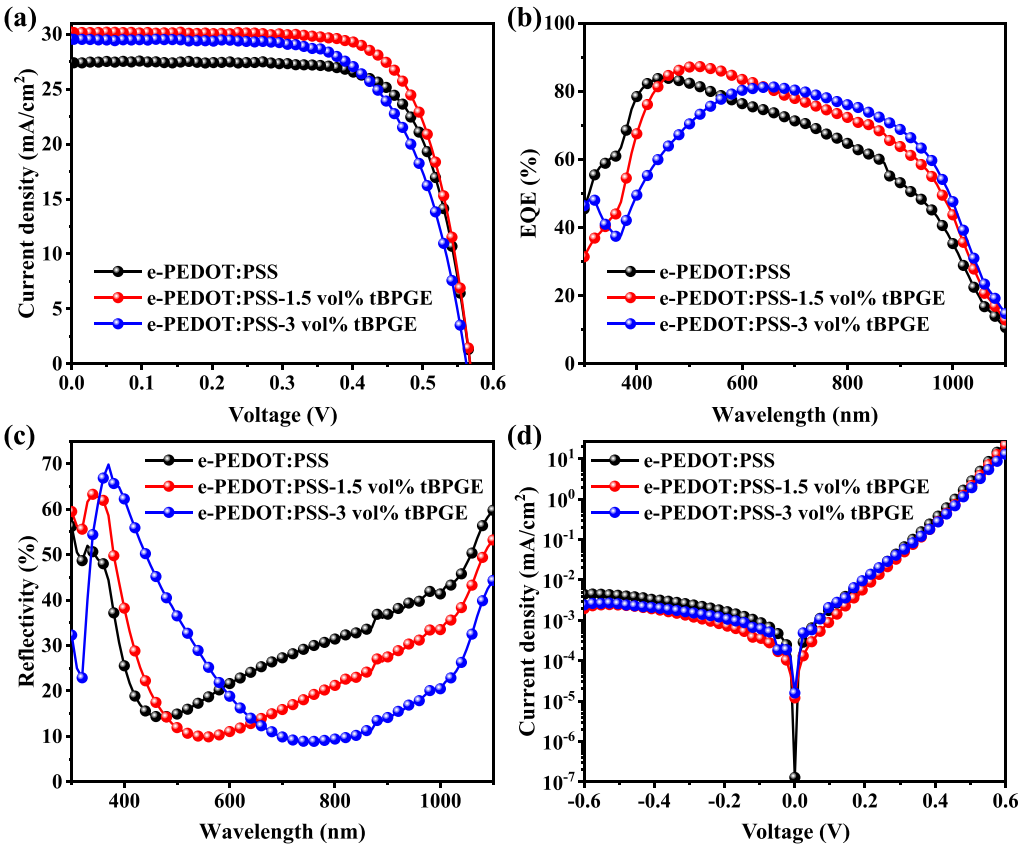

Figure 6. Performance of e-PEDOT:PSS/Si hybrid solar cells with different *t*BPGE doping concentrations. (a) *J*−*V* curves, (b) EQE spectra, (c) reflectivity spectra, and (d) *J*−*V* curves under dark conditions of e-PEDOT:PSS/Si hybrid solar cells with different *t*BPGE doping concentrations.

is 40.096 Ω/cm. Therefore, the conductivity of the film can be obtained by formula 1 as follows:

$$\sigma = \frac{1}{\rho \times A \times h} \quad (1)$$

where σ is the electric conductivity of the film, A is the length of the silver grid line (1.7 cm), and h is the thickness of the films (e-PEDOT:PSS film is 77.4 nm, and *t*BPGE-doped e-PEDOT:PSS film is 81.4 nm), as shown in Figure S5c,d. The electric conductivity of the *t*BPGE-doped e-PEDOT:PSS film reached 1802.26 S/cm, compared to 1685.16 S/cm for the undoped sample, as shown in Figure 4c. To elucidate this improvement, Raman spectra were analyzed, as shown in Figure 4d. The peaks between 1400 and 1500 cm^{-1} correspond to the $C_\alpha = C_\beta$ symmetric stretching in the five-member ring of PEDOT.[39] The *t*BPGE-doped e-PEDOT:PSS film shows a shift from 1430 cm^{-1} to 1413 cm^{-1} compared with the pristine e-PEDOT:PSS film. This result indicates that the doping of *t*BPGE promotes the packing of PEDOT chains,[39−41] leading to enhanced film conductivity.

3.3. Application in Si Hybrid Solar Cells. Based on the above analysis, *t*BPGE doping effectively weakens the

https://doi.org/10.1021/acsami.5c14719
ACS Appl. Mater. Interfaces 2025, 17, 62022−62031

Table 3. Electrical Output Parameters of e-PEDOT:PSS/Si Hybrid Solar Cells[a]

type	J_{SC} (mA/cm^2)	V_{OC} (mV)	FF (%)	PCE (%)
e-PEDOT:PSS	27.43 (27.39 ± 0.48)	567.25 (568.17 ± 2.37)	72.39 (71.40 ± 1.60)	11.26 (11.11 ± 0.34)
e-PEDOT:PSS-1.5 vol % *t*BPGE	30.20 (30.10 ± 0.33)	567.25 (567.70 ± 3.09)	71.86 (71.21 ± 0.67)	12.31 (12.16 ± 0.13)
e-PEDOT:PSS-3 vol % tBPGE	29.54 (29.22 ± 0.22)	562.55 (568.17 ± 5.03)	65.69 (66.24 ± 1.24)	10.92 (10.99 ± 0.26)

[a]The statistical data are from five sets of solar cell data.

hygroscopicity of the e-PEDOT:PSS film via nucleophilic ring-opening reactions, thereby attenuating both the changes in the film structure and the growth of the SiO_X. To explore the feasibility of this strategy to construct stable photovoltaic devices, we used the e-PEDOT:PSS films with and without *t*BPGE doping to fabricate Si hybrid solar cells. The devices were stored in different environments of a dry air atmosphere and ambient air to monitor the change of performance. The normalized PCE of the devices in a dry air atmosphere is shown in Figure 5a. It was found that, in Table 1, the initial PCE of the device without *t*BPGE doping was 11.26%; after 500 h, the device without *t*BPGE doping retained 61% of the initial efficiency, while the *t*BPGE-doped device retained 96% of the initial efficiency of 12.06%, which is a 57.3% increase in stability compared to the undoped device. In Figure 5b, after storage in ambient air for 500 h, the normalized PCE of the undoped device retained only 27% of its initial efficiency, while the *t*BPGE-doped device retained 77% of its initial efficiency of 12.31% in Table 2, which is a 185.1% increase in stability compared to the undoped device. In Figure 5c,d, we observed that the normalized FF and PCE of the devices exhibit parallel degradation trends in different environments. As shown in Figure 5e,f, the normalized V_{OC} and J_{SC} exhibited almost no degradation. To further demonstrate the potential of our strategy for practical application, the devices were further stored under about 35−40% humidity conditions. The normalized PCE of the devices is shown in Figure S6. It was found that in Table S4, the undoped device retained only 18% of the initial efficiency, while the *t*BPGE-doped device retained 72% of the initial efficiency after storage for 120 h. After the comparison of the stability of the devices in different humidity conditions, the *t*BPGE-doped device shows a satisfactory result, confirming the effectiveness of this strategy.

Finally, we investigated the impact of *t*BPGE doping on the performance of the e-PEDOT:PSS/Si hybrid solar cells. In Figure 6a, the devices doped with 1.5 vol % *t*BPGE achieved a J_{SC} of 30.20 mA/cm^2 compared to 27.43 mA/cm^2 for the undoped devices, and the FF and V_{OC} almost remained unchanged. The improvement in J_{SC} is mainly attributed to the increase in film conductivity. Therefore, the PCE achieved an improvement from 11.26% to 12.31%, as shown in Table 3. The EQE and reflectivity spectra of the devices are shown in Figure 6b,c. It was found that the EQE response was better than that of the undoped devices over the wavelength range from 500 to 1000 nm, and the reflectivity was lower than that of the undoped devices. As shown in Figure 6d, the dark $J-V$ curves exhibited no obvious gaps, but the device doped with 1.5 vol % *t*BPGE was still the best. However, a significant decrease in the FF of the device (from 71.86% to 65.69%) occurs with the increase in *t*BPGE doping (from 1.5 to 3 vol %), which leads to a decrease in the PCE of the device from 12.31% to 10.92% in Table 3. We further measured the Raman spectra of the e-PEDOT:PSS film at the condition of 3 vol % *t*BPGE doping, which found an obvious blue shift from 1413 cm^{-1} to 1435 cm^{-1} in Figure S7. It may cause the decrease in the conductivity of the e-PEDOT:PSS film, which further causes the decrease in FF and PCE of the device. According to the above study, the hygroscopicity of the e-PEDOT:PSS film was effectively weakened by *t*BPGE doping into e-PEDOT:PSS solution, and the storage stability of the device was also enhanced. But when applying this strategy to the fabrication process of photovoltaic devices, we need to ensure that the performance of photovoltaic devices is not damaged.

4. CONCLUSIONS

The hygroscopicity of e-PEDOT:PSS was successfully weakened through *t*BPGE incorporation, which undergoes ring-opening reactions, forming the C−O bonds between the carbon atom of the epoxy group and the oxygen atom of the sulfonic acid groups in PSS, successfully locking the hygroscopic sulfonic acid groups. The emerging chemical signals of six carbons in the ^{13}C NMR spectra (72.56, 71.69, 70.39, 70.24, 70.03, and 67.87 ppm) confirmed two ring-opening pathways of *t*BPGE. The peak intensity of surface SiO_X of the e-PEDOT:PSS film with *t*BPGE doping was lower than that of the undoped system after storage in air for 500 h. Through *t*BPGE doping, the electric conductivity of the e-PEDOT:PSS film was 1802.26 S/cm. Therefore, e-PEDOT:PSS/Si hybrid solar cells achieved a PCE of 12.31% compared to 11.26% without *t*BPGE. In a dry air atmosphere, the *t*BPGE-doped device exhibited a 57.3% stability enhancement compared to the undoped device. Meanwhile, in ambient air, the stability enhancement reached 185.1%, demonstrating long-term stability. This study not only gives a strategy that weakens the hygroscopicity of PEDOT:PSS for solving the stability of PEDOT:PSS/Si hybrid solar cells but also provides a potentially universal solution to reply to the inherent hygroscopicity challenge of PEDOT:PSS. It is expected to offer new insights for constructing a range of high-performance and stable PEDOT:PSS-based optoelectronic devices (such as perovskite tandem solar cells or OLEDs).

■ ASSOCIATED CONTENT

Supporting Information

The Supporting Information is available free of charge at https://pubs.acs.org/doi/10.1021/acsami.5c14719.

Normalized photovoltaic parameter curves, $J-V$ curves, and electrical output parameters of PEDOT:PSS/Si hybrid solar cells in a dry air atmosphere and ambient air; performance parameter curves and electrical output parameters of PEDOT:PSS/Si and e-PEDOT:PSS/Si hybrid solar cells; ^{13}C NMR spectra of e-PEDOT:PSS; and resistance and thickness of different films (PDF)

■ AUTHOR INFORMATION

Corresponding Author

Meicheng Li − *State Key Laboratory of Alternate Electrical Power System with Renewable Energy Sources, School of New Energy, North China Electric Power University, Beijing*

https://doi.org/10.1021/acsami.5c14719
ACS Appl. Mater. Interfaces 2025, 17, 62022−62031

*102206, China; orcid.org/0000-0002-0731-741X; Email: mcli@ncepu.edu.cn

Authors

Yuzhou Liu − *State Key Laboratory of Alternate Electrical Power System with Renewable Energy Sources, School of New Energy, North China Electric Power University, Beijing 102206, China*

Qi Geng − *State Key Laboratory of Alternate Electrical Power System with Renewable Energy Sources, School of New Energy, North China Electric Power University, Beijing 102206, China*

Zhe Wang − *State Key Laboratory of Alternate Electrical Power System with Renewable Energy Sources, School of New Energy, North China Electric Power University, Beijing 102206, China*

Zhen Liu − *State Key Laboratory of Alternate Electrical Power System with Renewable Energy Sources, School of New Energy, North China Electric Power University, Beijing 102206, China*

Zhongliang Gao − *School of Electrical and Electronic Engineering, Shandong University of Technology, Zibo 255000, China; orcid.org/0000-0001-8211-9985*

Xin Sun − *State Key Laboratory of Alternate Electrical Power System with Renewable Energy Sources, School of New Energy, North China Electric Power University, Beijing 102206, China*

Yingfeng Li − *State Key Laboratory of Alternate Electrical Power System with Renewable Energy Sources, School of New Energy, North China Electric Power University, Beijing 102206, China*

Complete contact information is available at: https://pubs.acs.org/10.1021/acsami.5c14719

Author Contributions

[§]Y.L. and Q.G. contributed equally. The manuscript was written through contributions of all authors. All authors have given approval to the final version of the manuscript.

Notes

The authors declare no competing financial interest.

■ ACKNOWLEDGMENTS

This work is supported partially by the National Natural Science Foundation of China (Grant nos. 52232008, 52302250, and 62304125), the Beijing Natural Science Foundation (2222076), the Hebei Natural Science Foundation (B2024502013), the project of China Three Gorges Corporation named key technologies of intelligent joint regulation and operation with grid connected friendly in power station group of wind, solar photovoltaic and energy storage (WWKY-2021-0173), the Huaneng Group Headquarters Science and Technology Project (HNKJ20-H88), the Fundamental Research Funds for the Central Universities (2025MS046, 2023MS042, 2023MS047), and the NCEPU "Double First-Class" Program.

■ REFERENCES

(1) Deng, J.; Gao, Y.; Che, Y.; Wang, X.; Sun, J.; Liao, Z.; Wang, X.; Li, Y.; Li, X.; Zhang, J.; Zhang, X.; Yang, L. Acid Doping of PEDOT:PSS Strengthens Interfacial Compatibility toward Efficient and Stable Perovskite Solar Cells. *ACS Appl. Energy Mater.* **2024**, *7* (20), 9577−9585.

(2) Li, S.; Cao, Y.-L.; Li, W.-H.; Bo, Z.-S. A brief review of hole transporting materials commonly used in perovskite solar cells. *Rare Met.* **2021**, *40* (10), 2712−2729.

(3) Zheng, Z.; Wang, J.; Bi, P.; Ren, J.; Wang, Y.; Yang, Y.; Liu, X.; Zhang, S.; Hou, J. Tandem Organic Solar Cell with 20.2% Efficiency. *Joule* **2022**, *6* (1), 171−184.

(4) Xu, J.; Heumüller, T.; Le Corre, V. M.; Barabash, A.; Félix, R.; Frisch, J.; Bär, M.; Brabec, C. J. A polymer bilayer hole transporting layer architecture for high-efficiency and stable organic solar cells. *Joule* **2024**, *8* (9), 2570−2584.

(5) Kayser, L. V.; Lipomi, D. J. Stretchable Conductive Polymers and Composites Based on PEDOT and PEDOT:PSS. *Adv. Mater.* **2019**, *31* (10), 1806133.

(6) Kim, T. G.; Ha, S. R.; Choi, H.; Uh, K.; Kundapur, U.; Park, S.; Lee, C. W.; Lee, S.-h.; Kim, J.; Kim, J.-M. Polymerizable Supramolecular Approach to Highly Conductive PEDOT:PSS Patterns. *ACS Appl. Mater. Interfaces* **2017**, *9* (22), 19231−19237.

(7) Zhang, W.; Zhao, B.; He, Z.; Zhao, X.; Wang, H.; Yang, S.; Wu, H.; Cao, Y. High-efficiency ITO-free polymer solar cells using highly conductive PEDOT:PSS/surfactant bilayer transparent anodes. *Energy Environ. Sci.* **2013**, *6* (6), 1956−1964.

(8) Mengistie, D. A.; Ibrahem, M. A.; Wang, P.-C.; Chu, C.-W. Highly Conductive PEDOT:PSS Treated with Formic Acid for ITO-Free Polymer Solar Cells. *ACS Appl. Mater. Interfaces* **2014**, *6* (4), 2292−2299.

(9) Lee, I.; Kim, G. W.; Yang, M.; Kim, T.-S. Simultaneously Enhancing the Cohesion and Electrical Conductivity of PEDOT:PSS Conductive Polymer Films using DMSO Additives. *ACS Appl. Mater. Interfaces* **2016**, *8* (1), 302−310.

(10) Kurushima, Y.; Katsuyama, N.; Okuzaki, H. Effect of PEDOT:PSS composition on photovoltaic performance of PEDOT:PSS/n-Si hybrid solar cells. *Jpn. J. Appl. Phys.* **2021**, *60* (9), 091001.

(11) Kawano, K.; Pacios, R.; Poplavskyy, D.; Nelson, J.; Bradley, D. D. C.; Durrant, J. R. Degradation of organic solar cells due to air exposure. *Sol. Energy Mater. Sol. Cells* **2006**, *90* (20), 3520−3530.

(12) Liu, H.; Liu, Q.; Liu, J.; Zhao, Y.; Yu, Y.; An, Y.; Wei, G.; Li, Y.; Fu, Y.; Li, J.; He, D. Effects of different interface on the stability of hybrid heterojunction solar cells. *Sol. Energy Mater. Sol. Cells* **2024**, *264*, 112624.

(13) Bießmann, L.; Kreuzer, L. P.; Widmann, T.; Hohn, N.; Moulin, J.-F.; Müller-Buschbaum, P. Monitoring the Swelling Behavior of PEDOT:PSS Electrodes under High Humidity Conditions. *ACS Appl. Mater. Interfaces* **2018**, *10* (11), 9865−9872.

(14) Oechsle, A. L.; Schöner, T.; Deville, L.; Xiao, T.; Tian, T.; Vagias, A.; Bernstorff, S.; Müller-Buschbaum, P. Ionic Liquid-Induced Inversion of the Humidity-Dependent Conductivity of Thin PEDOT:PSS Films. *ACS Appl. Mater. Interfaces* **2023**, *15* (40), 47682−47691.

(15) He, J.; Gao, P.; Ling, Z.; Ding, L.; Yang, Z.; Ye, J.; Cui, Y. High-Efficiency Silicon/Organic Heterojunction Solar Cells with Improved Junction Quality and Interface Passivation. *ACS Nano* **2016**, *10* (12), 11525−11531.

(16) He, J.; Gao, P.; Yang, Z.; Yu, J.; Yu, W.; Zhang, Y.; Sheng, J.; Ye, J.; Amine, J. C.; Cui, Y. Silicon/Organic Hybrid Solar Cells with 16.2% Efficiency and Improved Stability by Formation of Conformal Heterojunction Coating and Moisture-Resistant Capping Layer. *Adv. Mater.* **2017**, *29* (15), 1606321.

(17) Jiang, L.; Zhou, Z.; Zhang, G.; Li, C.; Feng, Q.; Wei, Q.; Li, J.; Wu, H.; Shi, Y.; Wang, J.; Yang, Y. Waterborne Acrylic Resin-Modified PEDOT:PSS as a Hole-Transporting Layer for Silicon/Organic Solar Cells with Improved Efficiency and Stability. *ACS Appl. Energy Mater.* **2024**, *7* (9), 3927−3936.

(18) Shen, R.; Sun, Z.; Zhou, Y.; Shi, Y.; Shang, J.; Chen, H.; Zhou, Y.; Liu, F. Organic/silicon nanowires hybrid solar cells using isobutyltriethoxysilane incorporated poly(3,4-ethylenedioxythiophene):poly (styrenesulfonate) as hole transport layer. *Prog. Photovolt.: Res. Appl.* **2022**, *30* (6), 661−669.

(19) Geng, Q.; Liu, Z.; Liu, Y.; Wang, Z.; Gao, Z.; Sun, X.; Li, Y.; Chen, L.; Lv, X.; Li, M. Air-stable silicon hybrid solar cells constructed via hydrophobic polymer film. *J Materiomics.* **2025**, *11* (3), 100935.
(20) Jiang, Y.; Dong, X.; Sun, L.; Liu, T.; Qin, F.; Xie, C.; Jiang, P.; Hu, L.; Lu, X.; Zhou, X.; Meng, W.; Li, N.; Brabec, C. J.; Zhou, Y. An alcohol-dispersed conducting polymer complex for fully printable organic solar cells with improved stability. *Nat. Energy* **2022**, *7* (4), 352−359.
(21) de Jong, M. P.; van Ijzendoorn, L. J.; de Voigt, M. J. A. Stability of the interface between indium-tin-oxide and poly(3,4-ethylenedioxythiophene)/poly(styrenesulfonate) in polymer light-emitting diodes. *Appl. Phys. Lett.* **2000**, *77* (14), 2255−2257.
(22) Abdul Jaleel, S. A.; Kim, T.; Baik, S. Covalently Functionalized Leakage-Free Healable Phase-Change Interface Materials with Extraordinary High-Thermal Conductivity and Low-Thermal Resistance. *Adv. Mater.* **2023**, *35* (30), 2300956.
(23) Brocas, A.-L.; Mantzaridis, C.; Tunc, D.; Carlotti, S. Polyether synthesis: From activated or metal-free anionic ring-opening polymerization of epoxides to functionalization. *Prog. Polym. Sci.* **2013**, *38* (6), 845−873.
(24) Kim, K.; Kim, M.; Lee, H.; Chung, D.-w.; Kim, J. Multi-Functional PEDOT:PSS as the Efficient Perovskite Solar Cells. *Small* **2024**, *20* (38), 2402341.
(25) Royappa, A. T.; McDaniel, R. L. Copolymerization of glycidol with functionalized phenyl glycidyl ethers. *J. Appl. Polym. Sci.* **2005**, *97* (4), 1462−1466.
(26) Jahanshahi, S.; Pizzi, A.; Abdulkhani, A.; Doosthoseini, K.; Shakeri, A.; Lagel, M. C.; Delmotte, L. MALDI-TOF, ^{13}C NMR and FT-MIR analysis and strength characterization of glycidyl ether tannin epoxy resins. *Ind. Crops Prod.* **2016**, *83*, 177−185.
(27) Babij, N. R.; McCusker, E. O.; Whiteker, G. T.; Canturk, B.; Choy, N.; Creemer, L. C.; Amicis, C. V. D.; Hewlett, N. M.; Johnson, P. L.; Knobelsdorf, J. A.; Li, F.; Lorsbach, B. A.; Nugent, B. M.; Ryan, S. J.; Smith, M. R.; Yang, Q. NMR Chemical Shifts of Trace Impurities: Industrially Preferred Solvents Used in Process and Green Chemistry. *Org. Process Res. Dev.* **2016**, *20* (3), 661−667.
(28) Suguna Lakshmi, M.; Reddy, B. S. R. Synthesis and characterization of new epoxy and cyanate ester resins. *Eur. Polym. J.* **2002**, *38* (4), 795−801.
(29) Jain, P.; Choudhary, V.; Varma, I. K. Effect of structure on thermal behaviour of epoxy resins. *Eur. Polym. J.* **2003**, *39* (1), 181−187.
(30) Yang, Z.; Li, N.; Yang, X.-x.; Zhang, X.-a.; Jiang, S.-l.; Lyu, Y.-f. Synthesis and characterization of carborane-containing poly(hydroxy ethers) with excellent thermal stability. *Chin. J. Polym. Sci.* **2017**, *35* (12), 1463−1473.
(31) Thi Khuat, K.-V.; Doan, H. N.; Vo, P. P.; Nguyen, D.; Kinashi, K.; Sakai, W.; Tsutsumi, N. Lightweight, flexible, and conductive PEDOT:PSS coated polyimide nanofibrous aerogels for piezoresistive pressure sensor application. *J. Mater. Chem. C* **2024**, *12* (20), 7240−7251.
(32) Han, M. G.; Foulger, S. H. Crystalline Colloidal Arrays Composed of Poly(3,4-ethylenedioxythiophene)-Coated Polystyrene Particles with a Stop Band in the Visible Regime. *Adv. Mater.* **2004**, *16* (3), 231−234.
(33) Suganuma, S.; Nakajima, K.; Kitano, M.; Yamaguchi, D.; Kato, H.; Hayashi, S.; Hara, M. Hydrolysis of Cellulose by Amorphous Carbon Bearing SO_3H, COOH, and OH Groups. *J. Am. Chem. Soc.* **2008**, *130* (38), 12787−12793.
(34) Nakajima, K.; Hara, M. Amorphous Carbon with SO_3H Groups as a Solid Brønsted Acid Catalyst. *ACS Catal.* **2012**, *2* (7), 1296−1304.
(35) Gong, C.; Luo, Q.; Li, Y.; Giotto, M.; Cipollini, N. E.; Yang, Z.; Weiss, R. A.; Scola, D. A. Dual crosslinked phenylethynyl end-capped sulfonated polyimides via the ethynyl and sulfonate groups promoted by PEG. *J. Polym. Sci., Part A: Polym. Chem.* **2011**, *49* (20), 4476−4491.
(36) Jäckle, S.; Liebhaber, M.; Niederhausen, J.; Büchele, M.; Félix, R.; Wilks, R. G.; Bär, M.; Lips, K.; Christiansen, S. Unveiling the Hybrid n-Si/PEDOT:PSS Interface. *ACS Appl. Mater. Interfaces* **2016**, *8* (13), 8841−8848.
(37) Sheng, J.; Fan, K.; Wang, D.; Han, C.; Fang, J.; Gao, P.; Ye, J. Improvement of the SiOx Passivation Layer for High-Efficiency Si/PEDOT:PSS Heterojunction Solar Cells. *ACS Appl. Mater. Interfaces* **2014**, *6* (18), 16027−16034.
(38) Morita, M.; Ohmi, T.; Hasegawa, E.; Kawakami, M.; Suma, K. Control factor of native oxide growth on silicon in air or in ultrapure water. *Appl. Phys. Lett.* **1989**, *55* (6), 562−564.
(39) Adilbekova, B.; Scaccabarozzi, A. D.; Faber, H.; Nugraha, M. I.; Bruevich, V.; Kaltsas, D.; Naphade, D. R.; Wehbe, N.; Emwas, A.-H.; Alshareef, H. N.; Podzorov, V.; Martín, J.; Tsetseris, L.; Anthopoulos, T. D. Enhancing the Electrical Conductivity and Long-Term Stability of PEDOT:PSS Electrodes through Sequential Treatment with Nitric Acid and Cesium Chloride. *Adv. Mater.* **2024**, *36* (41), 2405094.
(40) Ouyang, J. "Secondary doping" methods to significantly enhance the conductivity of PEDOT:PSS for its application as transparent electrode of optoelectronic devices. *Displays* **2013**, *34* (5), 423−436.
(41) Zhang, X.; Wu, J.; Wang, J.; Zhang, J.; Yang, Q.; Fu, Y.; Xie, Z. Highly conductive PEDOT:PSS transparent electrode prepared by a post-spin-rinsing method for efficient ITO-free polymer solar cells. *Sol. Energy Mater. Sol. Cells* **2016**, *144*, 143−149.

https://doi.org/10.1021/acsami.5c14719
ACS Appl. Mater. Interfaces 2025, 17, 62022−62031